

Critical properties of the three- and four-dimensional gauge glass

Helmut G. Katzgraber¹ and I. A. Campbell²

¹*Theoretische Physik, ETH Hönggerberg, CH-8093 Zürich, Switzerland*

²*Laboratoire des Verres, Université Montpellier II, 34095 Montpellier, France*

(Dated: May 22, 2019)

The gauge glass in dimensions 3 and 4 is studied using a variety of numerical methods, in order to obtain accurate and reliable values for the critical parameters. Detailed comparisons are made of the sensitivity of the different techniques to corrections to finite-size scaling, which are generally the major source of systematic error in such measurements. For completeness we also present results in two dimensions. The variation of the critical exponents with space dimension is compared to results in Ising spin glasses.

PACS numbers: 75.50.Lk, 75.40.Mg, 05.50.+q

I. INTRODUCTION

Spin glasses have long been recognized to be the canonical examples of complex systems and so of fundamental interest for statistical physics and in particular the statistical physics of phase transitions. The critical behavior at standard continuous transitions in systems *without* disorder is now understood very precisely and in impressive detail thanks to the renormalization group (RG) approach. An important step forward towards the comprehension of the vast family of glassy transitions would be to arrive at a similar degree of understanding concerning the critical behavior at the spin-glass transition. Unfortunately this task has proven to be extremely difficult. First of all, below the upper critical dimension ($d = 6$), the renormalization group theory that works so well for standard transitions has been found to present formidable technical difficulties¹ and is of little guidance in lower dimensions. Secondly, on the purely practical side, numerical work is laborious and has tended to lead to imprecise values of ordering temperatures and critical exponents. Randomly disordered samples are microscopically inequivalent to each other and to obtain data that are truly representative of the global average, measurements must be made over large numbers of disorder realizations. Time scales are long and obtaining thermal equilibrium in large system sizes is hard. Finite-size scaling methods are invariably used to estimate exponents but are carried out on a restricted range of sizes as the need for extensive computer time escalates when the system sizes increase. Because measurements are thus intrinsically restricted to small or moderate system sizes, it is essential to take into account possible artifacts due to corrections to finite-size scaling. Little is known about the magnitude of these corrections *a priori* and nevertheless the data must be analyzed in such a way that existing corrections are identified and allowed for.

Among spin glasses the Ising (ISG) systems have been by far the most studied numerically for obvious practical reasons. Here we report results using a variety of numerical techniques on the gauge glass (GG) in space dimensions $d = 3$ and 4. This system is of interest in its

own right because vector spin systems are generally much closer to experimental realizations of spin-glass ordering than are ISGs. Most laboratory spin glasses are made up of Heisenberg spins with $O(3)$ -symmetry and it has been suggested that chiral ordering plays an important role in spin freezing^{2,3}. Vortex glasses in type II superconductors can be modeled by XY vector spins [$O(2)$ symmetry], and GGs have already been studied extensively in this context^{4,5,6,7}. GGs are vector spin glasses which, due to symmetry arguments, do not show chiral ordering⁶.

This work has two main aims. The first is to take this particular family of spin glasses as a case study in order to demonstrate that there exists a whole toolbox of numerical techniques available to identify spin-glass ordering transitions and to attempt to estimate as reliably and precisely as possible the related critical exponents and the associated corrections to scaling. Each of these techniques can have its advantages and disadvantages, and we evaluate the reliability of the different methods. Second, having values for the GG exponents in hand which are as precise as possible, it is of interest to follow the evolution of their values as a function of space dimension in this particular family and to compare with values obtained in other families of spin glasses.

We have checked for and analyzed corrections to finite-size scaling in the observables measured; the relative influence of these corrections varies considerably from one observable to another. This can explain inconsistencies between the estimates of critical temperatures and critical exponents in various spin glasses which have been reported. We conclude that the “current” defined later (related to the domain-wall stiffness at low temperatures) is little affected by corrections to finite-size scaling and thus provides reliable estimates of the ordering temperature T_c . Measurements using the spin-glass susceptibility $\chi(L, T)$, alone or together with non-equilibrium measurements, are also accurate and reliable. On the other hand in the systems with finite-temperature transitions we have studied the intersection of the correlation length divided by system size, $\xi_L(T)/L$, and find that the method is very sensitive to corrections to finite-size scaling even for sizes where these corrections have be-

come negligible for other observables. This method on its own would give imprecise or misleading estimates for the ordering temperature of the GG. Nevertheless it can relatively well pinpoint if $T_c > 0$, or not, in general.

In Sec. II we introduce the model studied. In Sec. III we discuss the equilibration test used in the (parallel tempering) Monte Carlo method and describe the equilibrium observables measured. Off-equilibrium Monte Carlo methods and observables are discussed in Sec. IV, followed by results in $d = 4$ in Sec. V and $d = 3$ in Sec. VI. Some results for $d = 2$ are presented in Sec. VII. We conclude with a summary and a comparison of the techniques used to determine the critical parameters in Sec. VIII and with a discussion about the dimensional dependence of the critical exponents in Sec. IX. Concluding remarks are presented in Sec. X.

II. MODEL

The gauge glass is a canonical vector spin glass (see for instance Ref. 6) where XY spins on a [hyper]cubic lattice of size L interact through the Hamiltonian

$$\mathcal{H} = -J \sum_{\langle i,j \rangle} \cos(\phi_i - \phi_j - A_{ij}), \quad (1)$$

the sum ranging over nearest neighbors. The angles ϕ_i represent the orientations of the XY spins and the A_{ij} are quenched random variables uniformly distributed between $[0, 2\pi]$ with the constraint that $A_{ij} = -A_{ji}$. J is conventionally set equal to 1. Periodic boundary conditions are applied.

III. EQUILIBRIUM OBSERVABLES

Equilibrium measurements are carried out with samples fully thermalized using the exchange Monte Carlo (parallel tempering) technique^{8,9}. We ensure equilibration by checking that different observables do not change with the amount of Monte Carlo steps and measure by doubling the number of Monte Carlo steps. Once the last three measurements agree within error bars we are satisfied with the equilibration.

For XY spin systems there is a choice to be made in the allowed single-spin acceptance angle for individual updating steps. To optimize the updating procedure, the limiting angle is often chosen to be less than 2π for an XY spin¹⁰ and linearly dependent on temperature. The numerical pre-factor for the temperature-dependent window is chosen so that the acceptance ratios for the local Monte Carlo updates is ~ 0.4 . As far as the final equilibrium parameters are concerned, this choice plays no role. However, for the non-equilibrium simulations to be introduced later on it is important to use the full 2π acceptance angle.

In Table I, we show N_{samp} (number of samples), N_{sweep} (total number of sweeps performed by each set of spins),

TABLE I: Parameters of the equilibrium simulations in four dimensions. N_{samp} is the number of samples, N_{sweep} is the total number of Monte Carlo sweeps for each of the $2N_T$ replicas for a single sample, and N_T is the number of temperatures used in the parallel tempering method. $N_{\text{samp}}(\xi_L)$ is the total number of disorder realizations used in the calculation of the two-point correlation length ξ_L (defined below). The lowest temperature used is 0.70, the highest 1.345.

L	N_{samp}	$N_{\text{samp}}(\xi_L)$	N_{sweep}	N_T
3	5000	1660	2.0×10^4	17
4	5000	1250	8.0×10^4	17
5	5000	1000	4.0×10^5	17

TABLE II: Parameters of the equilibrium simulations in three dimensions. The lowest temperature simulated is 0.05, the highest 0.947. The different quantities are explained in the caption of Table I.

L	N_{samp}	$N_{\text{samp}}(\xi_L)$	N_{sweep}	N_T
3	10000	2660	6.0×10^3	53
4	10000	2000	2.0×10^4	53
5	10000	1600	6.0×10^4	53
6	5000	1330	2.0×10^5	53
8	2000	1000	1.2×10^6	53

and N_T (number of temperature values), used in the simulations in four dimensions. Table II has the corresponding values for the simulations in three dimensions. The parameters for the simulations in two dimensions are presented in Table III (see also Ref. 11).

A primary observable for a spin glass is the equilibrium spin-glass susceptibility at finite system size L , $\chi(L, T)$. The susceptibility is defined as¹²

$$\chi = N[\langle q^2 \rangle]_{\text{av}}, \quad (2)$$

where q is the spin-glass order parameter:

$$q = \frac{1}{N} \sum_{i=1}^N \exp[i(\phi_i^\alpha - \phi_i^\beta)]. \quad (3)$$

TABLE III: Parameters of the equilibrium simulations in two dimensions. The lowest temperature used is 0.13, the highest 1.058. For $L = 24$ the lowest temperature studied is 0.20. The different quantities are explained in the caption of Table I.

L	N_{samp}	$N_{\text{samp}}(\xi_L)$	N_{sweep}	N_T
4	10400	4000	8.0×10^4	30
6	10150	2660	8.0×10^4	30
8	8495	2000	2.0×10^5	30
12	6890	1330	8.0×10^5	30
16	2500	1000	2.0×10^6	30
24	2166	–	2.0×10^6	24

Here, α and β are two replicas of the system with the same disorder and $[\cdots]_{\text{av}}$ represents a disorder average, whereas $\langle \cdots \rangle$ represents a thermal average; N is the number of spins in the system. The standard finite-size scaling form for the equilibrium spin-glass susceptibility is

$$\chi(L) = L^{2-\eta} \tilde{C}[L^{1/\nu}(T - T_c)] . \quad (4)$$

The function \tilde{C} tends to a constant at the critical temperature so that at T_c

$$\chi(L) \propto L^{2-\eta} , \quad (5)$$

where η and ν are the usual critical exponents. Following the RG approach, the spin-glass susceptibility, like the other observables, will be modified at small L by a correction to scaling factor $\sim [1 + AL^{-\omega} + \dots]$, where ω is the correction exponent arising from the leading irrelevant operator in the RG and A is a constant. However, in general there are also “lattice artifact” correction terms¹³ giving at T_c

$$\chi(L) \propto L^{2-\eta} + B + \dots , \quad (6)$$

where B has no relation to the RG correction. This leads to an effective leading correction factor $[1 + B'L^{-(2-\eta)}]$. If $\omega > (2 - \eta)$ corrections will be dominated by the leading “analytic” term with an effective correction exponent $(2 - \eta)^{13,14,15}$.

Spin-glass susceptibility measurements can be used directly to estimate T_c . As $\chi(L)$ in absence of corrections to scaling increases as $L^{2-\eta}$ at the ordering temperature, a log-log plot of $\chi(L)$ against L is linear at T_c . At higher temperatures the plot will curve downward and at lower temperatures it will curve upward. The crossover from negative to positive curvature at large L should give a precise measure of T_c . Alternatively one can plot $\ln[\chi(nL)/\chi(L)]$ as functions of T for different L , and, for instance, $n = 2$. The curves will intersect at T_c . Direct scaling of $\chi(L, T)$ according to Eq. (4) on the contrary provides a very poor indication for T_c ⁷. In presence of corrections there will be an additional curvature at small L which should be essentially temperature independent near T_c . If data on a reasonably wide range of L are available it is possible to identify the leading correction term and to estimate T_c using data at L -values large enough for the correction term to be negligible.

The Binder ratio¹⁶ for the GG is defined by¹⁷

$$g(T) = 2 - \frac{[\langle q^4 \rangle]_{\text{av}}}{[\langle q^2 \rangle]_{\text{av}}^2} . \quad (7)$$

Finite-size scaling predicts

$$g(T, L) = \tilde{G}[L^{1/\nu}(T - T_c)] . \quad (8)$$

This dimensionless observable should be independent of L at T_c , except for corrections to scaling. The Binder ratio is a *bona fide* “work horse” widely used to obtain an estimate of the critical temperature of statistical systems.

It has frequently been used in ISG studies to estimate ordering temperatures. However, even in ISGs the Binder crossing point method is not efficient for determining T_c precisely, at least in dimension 3, because the $g(T, L)$ curves tend to lie very close to each other so the estimate of the crossing point is very sensitive to corrections to scaling¹⁸. In the particular case of the GG, the method is inoperable because the Binder curves do not intersect, at least for the range of sizes that have been studied here.

For vector systems it is possible to measure a domain-wall-stiffness like parameter, the “current”^{4,5,6,7}, which is the rate of change of the free energy with respect to a twist angle at the boundaries. For the gauge glass:

$$I(L) = \frac{1}{L} \sum_{i=1}^N \sin(\phi_i - \phi_{i+\hat{x}} - A_{i,i+\hat{x}}) . \quad (9)$$

In this case, the twist is applied along the \hat{x} -direction. As $[\langle I(L) \rangle]_{\text{av}} = 0$, we actually calculate the root-mean-square current I_{rms} between two replicas:

$$I_{\text{rms}} = \sqrt{[\langle I(L)_\alpha \rangle \langle I(L)_\beta \rangle]_{\text{av}}} . \quad (10)$$

The root-mean-square currents for different L cross at T_c and splay out at lower temperatures. They have a finite-size scaling form for a finite-temperature transition⁷

$$I = \tilde{I}[L^{1/\nu}(T - T_c)] . \quad (11)$$

The intersection of the $I_{\text{rms}}(L)$ curves gives a clear indication of the value of T_c . Corrections to finite-size scaling must be allowed for, but in practice these are weak. The main drawback of this method is the fact that in current measurements intrinsic sample to sample fluctuations are very strong so that data must be taken on a large number of independent disorder realizations in thermal equilibrium.

A further important observable is the two-point correlation length. In an infinite sample the correlation function

$$G(r_{ij}) = [\langle \mathbf{S}_i \cdot \mathbf{S}_j \rangle^2]_{\text{av}} \quad (12)$$

is of the form

$$G(r_{ij}) \propto r_{ij}^{-(d-2+\eta)} e^{-r_{ij}/\xi(T)} , \quad (13)$$

where i and j represent the position of the magnetic moments. $\xi(T)$ is the correlation length, which diverges as $(T - T_c)^{-\nu}$. In some systems $G(r)$ has been directly recorded; when T_c is known, the measurement of $G(r)$ at T_c on reasonably large samples provides a very direct measurement of η . (Measurements have also been made as a function of anneal time for temperatures lower than T_c in the Edwards Anderson ISG¹⁹). Under periodic boundary conditions there must clearly be a cutoff for $G(r)$ at $r_{ij} = L/2$, and even before this cutoff the behavior is modified as $G(r_{ij})$ must become r -independent

at the cell boundary so as to be compatible with the periodic boundary conditions. A size-dependent correlation length ξ_L can be defined through^{20,21,22,23}

$$\xi_L = \frac{1}{2 \sin(|\mathbf{k}_{\min}|/2)} \left[\frac{\hat{G}(\mathbf{0})}{\hat{G}(\mathbf{k}_{\min})} - 1 \right]^{1/2}, \quad (14)$$

where $\hat{G}(\mathbf{0})$ and $\hat{G}(\mathbf{k}_{\min})$ are Fourier transforms of the spatial correlation function $G(r)$ ²⁴ and $\mathbf{k}_{\min} = (2\pi/L, 0, 0)$ is the smallest nonzero wave vector. This second-moment correlation length is in fact an observable having the dimension of length, which becomes equal to the correlation length in the limit $L \gg \xi$. It is referred to as the “size-dependent correlation length” even in the limit of $T = T_c$ and below, where the infinite-size correlation length ξ has diverged. The ratio ξ_L/L at T_c should be L -independent¹¹ as the form of the whole function $G(r)$ scales appropriately with L . Curves for the ratio of the finite-size correlation length to sample length $\xi_L(T)/L$ for different L cross at T_c and then splay out at lower T ^{11,20,21,25}, i.e.,

$$\xi_L/L = \tilde{X}[L^{1/\nu}(T - T_c)]. \quad (15)$$

This makes this observable very attractive for estimating T_c . Unfortunately at small and moderate L , the ratio ξ_L/L can be very susceptible to corrections to scaling. In addition, the definition of ξ_L through Eq. (14) is a convention and other definitions having the same limiting form at infinite L are equally plausible¹³. At small and moderate L there are correction terms $\sim L^{-2}$ from the sub-leading term in the sine factor in the conventional definition. There may be a “lattice artifact” correction term¹³ of order $1/L$, in addition to the “true” correction term in $L^{-\omega}$ arising from the leading irrelevant operator. Physically, $\hat{G}(\mathbf{0})$ is the sum over the spins within a box $\sim L^d$ correlated to a central spin and so is equal to the equilibrium $\chi(L)$. $\hat{G}(2\pi/L)$ contains a positive term from spins close to the central spin together with a term from some of the spins further from the central spin which is negative because of the cosine factor. A slight change in the form of the function $G(r)$ with L will have little effect on the L -dependence of $\hat{G}(\mathbf{0})$ while it can modify the Fourier transform $\hat{G}(2\pi/L)$ much more drastically. Hence one can expect that at low and moderate L , ξ_L/L will be much more sensitive to corrections to finite-size scaling than $\chi(L)$ will. Even for the canonical ferromagnetic Ising model in two dimensions, the corrections in ξ_L/L (or to the variant second moment correlation length ξ'_L/L with a slightly different definition¹³) at criticality are strong for $L \leq 20$, with different correction terms contributing¹³. As a consequence, correlation-length data should as a general rule be treated with caution unless detailed results exist over a wide range of L from which the various correction contributions can be evaluated.

Taken over the entire temperature range, ratios such as $\xi_{2L}(T)/\xi_L(T)$ or $\chi(2L, T)/\chi(L, T)$ should be universal

scaling functions of $\xi_L(T)/L$ ²⁵. If there are corrections to scaling, scaling curves for different L will not be identical; this provides an operational method for checking for corrections to scaling in ξ_L/L not only at or near T_c , but over the whole range of temperatures.

Finally, we also record the equilibrium energy per spin. As is well known, the energy of glassy systems varies smoothly through the ordering temperature, but the size dependence of the energy has a behavior linked to the ordering temperature. This is discussed elsewhere²⁶.

IV. OUT OF EQUILIBRIUM METHODS

Complementary out-of-equilibrium measurements are also carried out. Large samples of size L are initialized in a disordered (infinite temperature) state; they are then held at a bath temperature T for an anneal time t_w . The spin-glass susceptibility $\chi(t, t_w)$ is monitored as a function of t . At T_c dynamic scaling rules hold; the spin-glass susceptibility increases proportional to $t^{(2-\eta/z)}$, as clusters of correlated spins build up over time²⁷. This equation is not valid at very short time scales as χ is identically equal to 1 for a sample of any size and dimension in the totally disordered state, so the scaling equation will only set in after a crossover from this initial zero-time value. Even after this crossover, there can be corrections to scaling in the non-equilibrium susceptibility data, when only small clusters have been built up. Here the corrections appear as corrections to *finite time* scaling but are physically equivalent to corrections to *finite-size* scaling. Including the correction term,

$$\chi(t) = At^{(2-\eta/z)}(1 + Bt^{-w/z} + \dots), \quad (16)$$

where w is a dynamic correction to scaling exponent analogous to ω ²⁸. In principle w and ω have no fundamental reason to be exactly equal but can be expected to be similar. Finally, if the measurement is continued long enough, the long-time susceptibility will cross over to a saturation value which is just the equilibrium susceptibility $\chi(L, T)$ for the measurement temperature T and the sample size L used.

It is clear from a comparison of the equations for the equilibrium susceptibility and the dynamic susceptibility at T_c that for all intermediate times between the very short time limit and the L -dependent long-time limit, the measurement after a time t_w on a large sample should be equivalent to the measurement at equilibrium on a sample of size

$$L^* = At^{1/z}, \quad (17)$$

with A a constant and z the dynamic scaling exponent. $\chi(L)$ and $\chi(L^*)$ can be displayed on the same graph; with a judicious choice of parameters $A(T)$ and $z(T)$ the set of $\chi(L^*)$ scale onto the set of equilibrium data $\chi(L)$. This provides us with a direct method for estimating $z(T)$. Alternative techniques which have been used for estimating

the value of $z(T)$ independently of the other exponents are the monitoring of the time variation of the Binder parameter for different sample sizes²⁹ or the scaling of the time-dependent spin-glass susceptibility $\chi(L, t)$ for different sizes L ⁶. The present method is more convenient than the Binder parameter measurements as the latter are intrinsically noisy.

We have carried out dynamical measurements over a range of temperatures and not just at the putative ordering temperature. If we assume that there is an effective dynamic scaling exponent $z(T)$ at each temperature T and not only at T_c , then at each T we should be able to translate $\chi(t)$ data into $\chi(L^*)$ data by a suitable choice of $A(T)$ and $z(T)$. If dynamic scaling continues to hold at other T , then once again it should be possible to make the $\chi(L^*)$ data scale onto the $\chi(L)$ data. The assumption of an effective $z(T)$ has been made before in a different context, but applied only at temperatures below T_c (see for instance Refs. 19 and 30).

Finally, after a long anneal time t_w the ultimate configuration $\{\mathbf{S}_i(t_w)\}$ is registered. The updating procedure is then pursued for a further time t considerably less than t_w and the autocorrelation function decay

$$q(t, t_w) = \frac{1}{N} \sum_{i=1}^N \langle \mathbf{S}_i(t_w + t) \cdot \mathbf{S}_i(t_w) \rangle \quad (18)$$

is monitored starting from what can now be considered a quasi-equilibrium configuration. In Eq. (18) \mathbf{S}_i represent the vector spins in the plane. In the context of Ising spin glasses it has been shown^{19,31,32} that the initial decay behavior of $q(t, t_w)$ is not dependent on the sample having achieved perfect thermal equilibrium; as long as the time scale over which $q(t, t_w)$ is monitored is much shorter than the annealing time t_w , then the form of $q(t, t_w)$ is characteristic of the infinite-size limit initial relaxation in equilibrium. Again at T_c , for a large sample in equilibrium, the autocorrelation function $q(t, t_w)$ decays algebraically as $q(t, t_w) \sim t^{-x}$ with³³

$$x = (d - 2 + \eta)/2z. \quad (T = T_c) \quad (19)$$

Measurements in Ising spin glasses^{19,31,32,34} have shown that at all temperatures below T_c the $q(t, t_w)$ data can be accurately fitted by this power-law form of decay with a temperature-dependent effective exponent $x(T)$. For temperatures higher than T_c , the decay of $q(t, t_w)$ has the same initial power-law form which is now multiplied by a further factor $\tilde{Q}(t/\tau(T))$, where \tilde{Q} is a scaling function and $\tau(T)$ is a relaxation time diverging as $(T - T_c)^{-z\nu}$ when T_c is approached from above³³. In ISG measurements $q(t, t_w)$ shows very little short-time corrections to scaling; at $T = T_c$ and below, $q(t, t_w)$ for large well-annealed samples follows a strict power-law decay beyond very few Monte Carlo steps after “zero” time.

Non-equilibrium measurements can be used in combination with the equilibrium susceptibility measurements to obtain an estimate of T_c from consistency arguments³⁵. The effective dynamical exponent $z(T)$ is measured from

TABLE IV: Parameters of the off-equilibrium simulations as a function of space dimension d . L is the size of the system used, t the equilibration time and t_w is the “waiting time” to calculate $q(t, t_w)$, Eq. (18). N_{samp} is the number of samples used for the disorder average.

d	L	N_{samp}	t	t_w
2	64	500	1.638×10^4	4.069×10^3
3	16	200	8.192×10^3	8.192×10^3
4	10	200	1.310×10^5	4.096×10^3

the comparison of equilibrium and non-equilibrium susceptibility measurements. The effective exponent $\eta(T)$ is measured from the size-dependent equilibrium susceptibility measurements through $\chi(L, T)/L^2 = L^{-\eta(T)}$. Then, at T_c , the relaxation decay exponent x must be equal to $(d - 2 + \eta)/2z$. The consistency between the directly measured $x(T)$ and the other exponents gives an efficient criterion for determining T_c . This technique has a number of advantages. $x(T)$ and $z(T)$ can be measured on almost arbitrarily large samples and so can be rendered free of corrections to scaling. In addition, they can be measured without the need to achieve complete thermal equilibrium. The most laborious measurement is the size-dependence of $\chi(T)$ in equilibrium; however, $\chi(L, T)$ measurements are generally only subject to weak corrections to finite-size scaling so a limited range of L can be adequate.

The parameters of the off-equilibrium simulations using simple Monte Carlo updates are listed in Table IV.

V. FOUR DIMENSIONS

In this section we compare different observables as well as critical exponents and transition temperatures derived from finite-size scaling arguments for the four-dimensional gauge glass.

A. Root-mean-square Current

Current measurements are made for sizes $L = 3 - 5$. The details of the simulation are shown in Table I. The intersection of the I_{rms} curves shown in Fig. 1 give an estimate $T_c = 0.890 \pm 0.015$. This is significantly lower than the value of 0.96 ± 0.01 reported by Reger and Young⁵, although their data are almost compatible with the present intersection point within the statistical error bars. Corrections to finite-size scaling appear to be minimal for these measurements. However, current measurements are intrinsically noisy with strong sample to sample variations at equilibrium, so it is imperative to average over large numbers of samples. In Fig. 2 we show a scaling plot of the data in Fig. 1 according to Eq. (11). The data scale well for the (modest) range of sizes and we estimate $1/\nu = 1.42 \pm 0.03$ together with the above

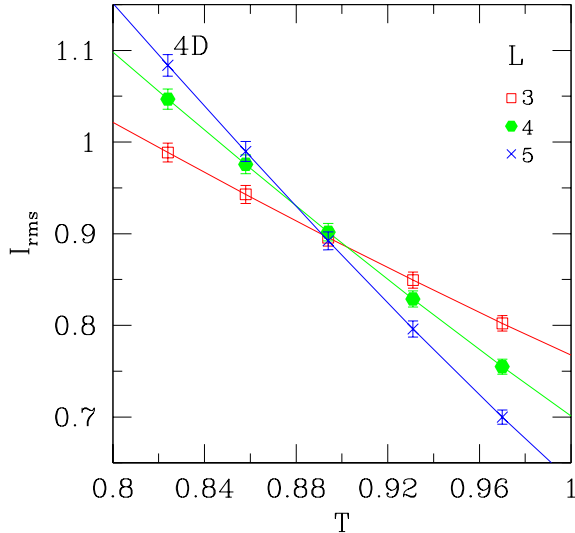


FIG. 1: Data for the the root-mean-square current I_{rms} in four dimensions. The data show a crossing at $T_c \approx 0.89$.

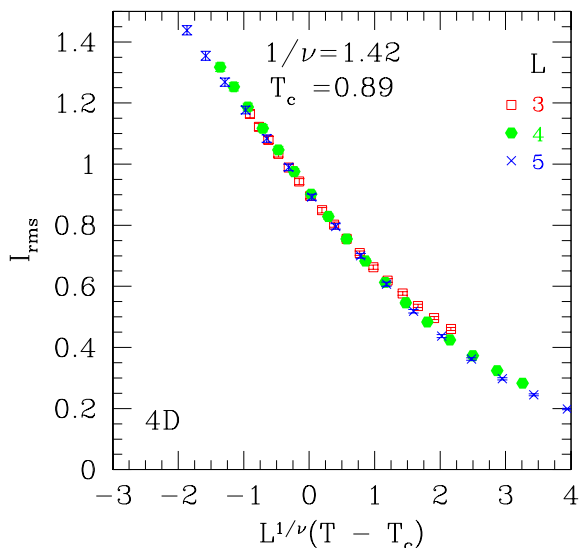


FIG. 2: Scaling of the root-mean-square current I_{rms} in four dimensions according to Eq. (11). The data scale well for the range of sizes shown and we estimate $1/\nu \approx 1.42$ with $T_c \approx 0.89$.

mentioned estimate of T_c . The previously quoted error is estimated by varying the scaling parameters until the data do not collapse well. This method is also used in all subsequent estimates of error bars of scaling exponents and critical temperatures derived from scaling plots.

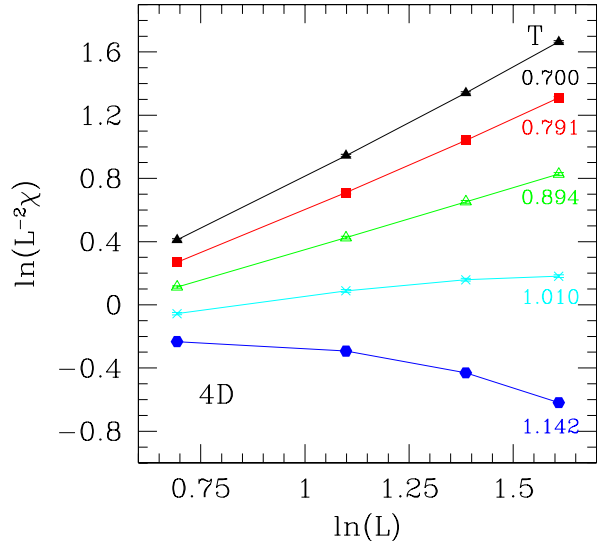


FIG. 3: Data for $\ln(\chi/L^2)$ vs $\ln(L)$ for different temperatures in four dimensions. At T_c one expects $\chi \sim L^{2-\eta}$. The data show a change in curvature while scanning through $T_c \approx 0.89$.

B. Equilibrium Susceptibility

The susceptibility data at equilibrium are obtained from the same data set in Sec. V A and shown in Fig. 3. The data are plotted in the form of curves for $\ln[\chi(L)/L^2]$ against $\ln L$ at different temperatures. As discussed above, if corrections to scaling are negligible, this form of plot gives a straight line of slope $-\eta$ at T_c , together with curves which bend downward for $T > T_c$ and upward for $T < T_c$. For the four-dimensional GG, corrections are very weak because even including values for $L = 2$ the log-log plot of the data at the temperature closest to T_c as estimated above follows the straight line behavior very closely.

In order to obtain an independent estimate for T_c , we have plotted the χ^2 -deviation from a straight line fit to the data over a range of temperatures around $T = 0.89$, together with the curvature for three-parameter fits, Figs. 4 and 5. The results indicate straight-line behavior for $T = 0.895 \pm 0.015$ which is an independent measurement of T_c . In Fig. 5 we also show the effective slope $-\eta(T)$ from the three-parameter fit. The slope of the straight line at T_c gives an estimate of the critical exponent $\eta = -0.74 \pm 0.03$. As far as we are aware of, this is the first published estimate for this parameter for the GG in four dimensions.

With values for T_c and η in hand, the whole $\chi(L, T)$ data set can be plotted in a standard manner: $\chi(L, T)/L^{2-\eta}$ as a function of $L^{1/\nu}(T - T_c)$, adjusting ν to obtain optimal scaling. The results lead to $1/\nu = 1.42 \pm 0.03$, as shown in Fig. 6, and in agreement with an estimate from the scaling of the currents presented in Fig. 2.

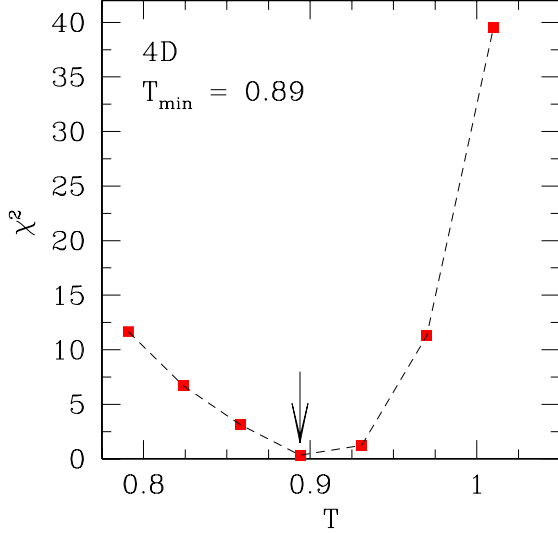


FIG. 4: χ^2 -deviation from a straight-line fit for the susceptibility data in four dimensions shown in Fig. 3. The data show a minimum at $T \approx 0.89$, indicating that the optimal fit happens around $T = T_c$ (marked by an arrow).

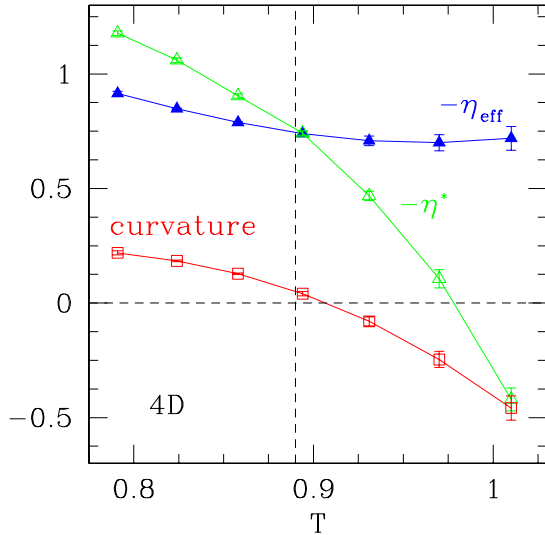


FIG. 5: Data for the effective exponent $\eta_{\text{eff}}(T)$ as a function of temperature in four dimensions. The vertical dashed line marks our estimate of T_c from current and susceptibility measurements, $T_c = 0.89$. In addition, η^* is shown, an effective exponent derived from off-equilibrium calculations (described in detail in Sec. IV). One expects η_{eff} and η^* to cross at T_c , which is the case in our data within error bars. Data for the curvature of the susceptibility shown in Fig. 3 from a second-order polynomial fit are also displayed. The data cross zero curvature (horizontal dashed line) at $T \approx 0.90$, a value slightly higher than the other estimates.

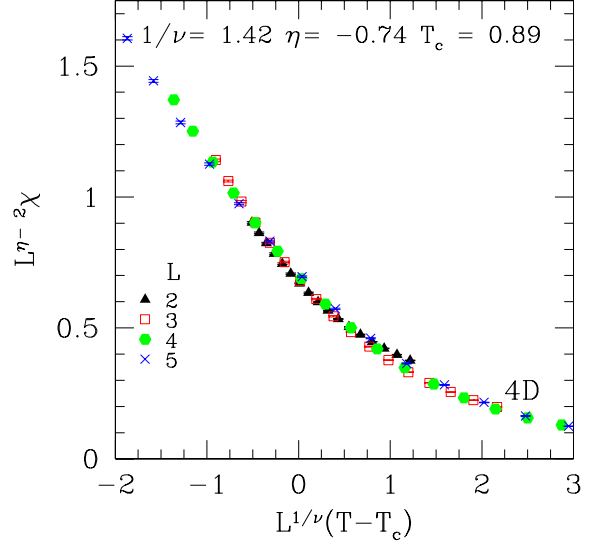


FIG. 6: Scaling plot according to Eq. (4) of the susceptibility data presented in Fig. 3 in four dimensions. The data scale well for $T_c \approx 0.89$, $1/\nu \approx 1.42$, and $\eta \approx -0.74$. Note that only the data for $L = 2$ show corrections to scaling.

C. Correlation length

The data for the ratio $\xi_L(T)/L$ for different sizes are shown in Fig. 7. Although the data appear to cleanly intersect at one point, it can be seen that the intersection temperatures for these sizes are around $T \approx 1.0$, and are only approaching the true ordering temperature, $T_c = 0.89$, very slowly with increasing L . The comparison with the behavior observed for $\chi(L)$ or the current is striking. For each of these two parameters the critical behavior at T_c is virtually correction-free, while for the same range of small values of L , the ξ_L/L intersections give a very poor indication of the true ordering temperature. There are clearly strong corrections to scaling at small L which appear to be intrinsic to this form of measurement.

D. Non-equilibrium susceptibility

Large samples ($L = 10$ in four dimensions) are initialized in random (infinite temperature) configurations. They are then put in contact with a heat bath at a temperature T , and the spin-glass susceptibility is recorded as a function of annealing time. At T_c the spin-glass susceptibility will increase as $t^{(2-\eta)/z}$ until the susceptibility arrives at the equilibrium value for that size L . We present the data in terms of the scaled time-dependent effective length $L^* = At^{1/z}$ at each temperature. When A and z are suitably chosen, the equilibrium susceptibility $\chi(L)$ and the non-equilibrium susceptibility $\chi(L^*)$ before saturation scale well together. An example for a temperature close to T_c , $T = 0.894$, is shown in Fig. 8.

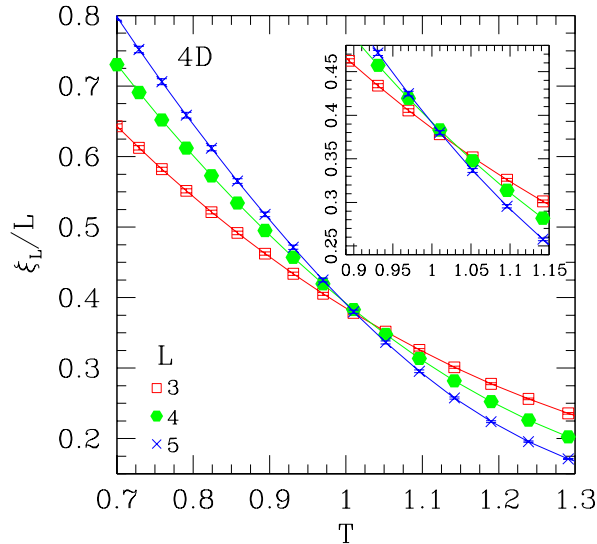


FIG. 7: Correlation length ξ_L divided by L for different system sizes in four dimensions. The data cross at $T \approx 1.0$ indicating that there are strong corrections to scaling. The inset shows a zoom of the data in the main panel focusing on the crossing point around $T \approx 1$.

From the data, the dynamical scaling exponent $z(T)$ can be determined accurately, see Fig. 9. The behavior of the effective dynamical exponent $z(T)$ shows no apparent special behavior at the critical temperature. Effective temperature-dependent values $z(T)$ have been reported in ISGs for $T < T_c$ (see for instance Ref. 30). We can conclude from the present data for the GG that $z(T)$ is a well-defined parameter for a whole range of temperatures including $T > T_c$. At $T = T_c$ we estimate $z = 4.50 \pm 0.05$.

E. Autocorrelation function decay

In the GG we have found unexpectedly that $q(t)$ only assumes a pure power-law behavior after a relatively long time, of the order of 100 MCS (as compared with ~ 5 MCS in ISGs), see Fig. 10. For earlier times the decay is affected by short-time corrections. In practice this means that the measurements of $x(T)$ as defined above are less precise than in ISGs as they are limited at short times by the correction term and at long times by the condition that the maximum t_w should be much less than t .

We compare, for a set of temperatures around T_c , the value of $\eta(T)$ directly obtained from the equilibrium susceptibility measurements with a value calculated indirectly from the $x(T)$ and $z(T)$ data, $\eta^*(T) = (d-2) - 2z(T)x(T)$. We expect $\eta(T) = \eta^*(T)$ at $T = T_c$. This can be seen in Fig. 5 where the vertical dashed line marks our estimate of T_c . The two curves cross at $T = 0.90 \pm 0.01$, $\eta = -0.74 \pm 0.02$, which again defines the ordering temperature and the critical exponent η . As for this particular system T_c is already reliably es-

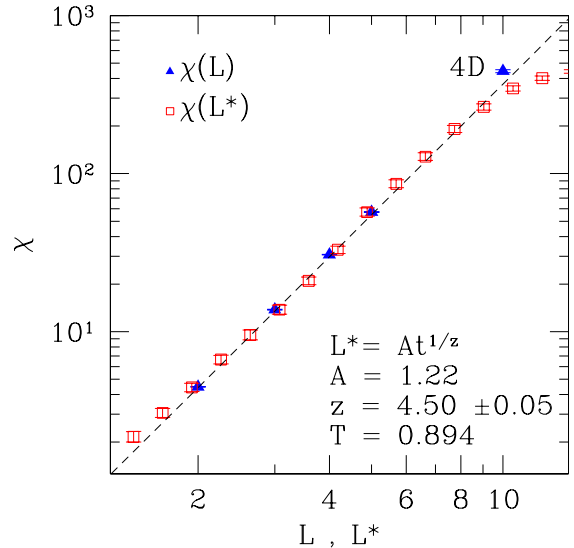


FIG. 8: Spin-glass susceptibility from equilibrium measurements $\chi(L)$ at $T = 0.894$ in four dimensions. $\chi(L^*)$ is the susceptibility determined from the off-equilibrium simulations with $L^* = At^{1/z}$, $A = 1.22$, and $z \approx 4.5$. By suitably choosing L^* the data for $\chi(L)$ and $\chi(L^*)$ fall on a straight line. This allows us to determine the dynamical critical effective exponent $z(T)$ as a function of temperature. When $L^*(t)$ approaches the sample size (here $L = 10$), $\chi(L^*)$ necessarily saturates. The dashed line is a guide to the eye.

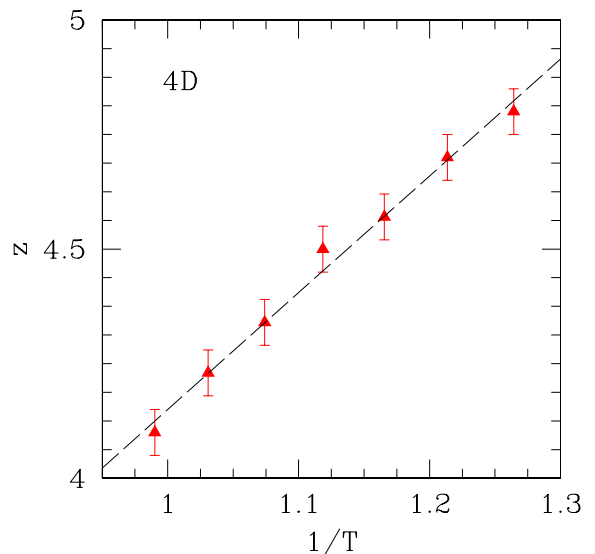


FIG. 9: Dynamical critical exponent z as a function of $1/T$ in four dimensions as determined from the procedure described in the text and in the caption of Fig. 8. The data are consistent with $z(T = T_c) = 4.50 \pm 0.05$. Note that the error is estimated “by eye”: the data are varied until the two expressions for the susceptibility differ noticeably thus allowing us to give an upper bound for the error bars. The dashed line is a guide to the eye.

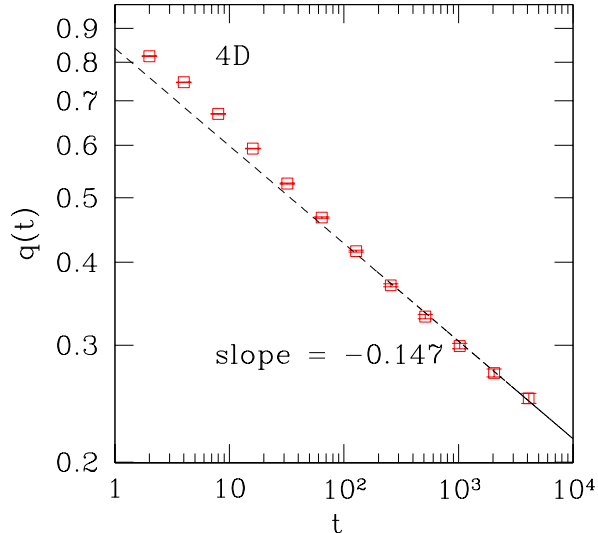


FIG. 10: Data for the autocorrelation function $q(t)$ in four dimensions as a function of time (measured in Monte Carlo steps). The dashed line has slope $-x = -0.147$ from which we can determine η^* , a “dynamical” effective exponent η . Details are described in the text.

tablished from the previously mentioned methods, the comparison provides a critical benchmark test for the non-equilibrium technique. The good agreement with the standard methods, such as susceptibility scaling, two-point correlation length crossing and the crossing of root-mean-square currents in this case shows that this method is reliable, implying that it can be used for other systems.

VI. THREE DIMENSIONS

A number of estimates have already been given of the ordering temperature and critical exponents of the GG in dimension three⁶. In this section we present estimates for the critical temperature and exponents as derived from our simulations. In comparison to the four-dimensional data presented in Sec. V we find strong corrections to scaling in three dimensions. In what follows the different results for different observables are presented.

A. Root-mean-square Current

Olson and Young⁶ estimated that $T_c = 0.47 \pm 0.03$ from the intersection of the root-mean-square current induced by an infinitesimal twist along the boundaries. The present current data are shown in Fig. 11. Our results agree with the data of Ref. 6 within error bars. A consistent intersection point for all the data taken together occurs at $T = 0.46 \pm 0.01$, with only the data for $L = 3$ lying slightly below the region of intersection. We conclude that this temperature indeed represents the cor-

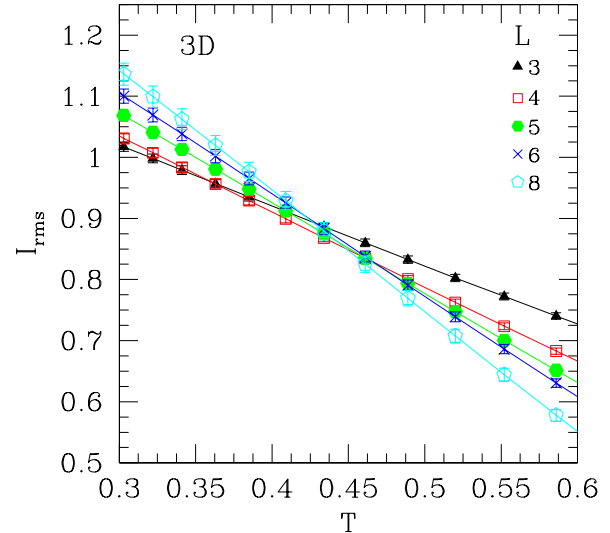


FIG. 11: Root-mean-square current I_{rms} as a function of temperature for the three-dimensional GG. The data show a crossing at $T \approx 0.46$. Note that the data for $L = 3$ show strong corrections to scaling.

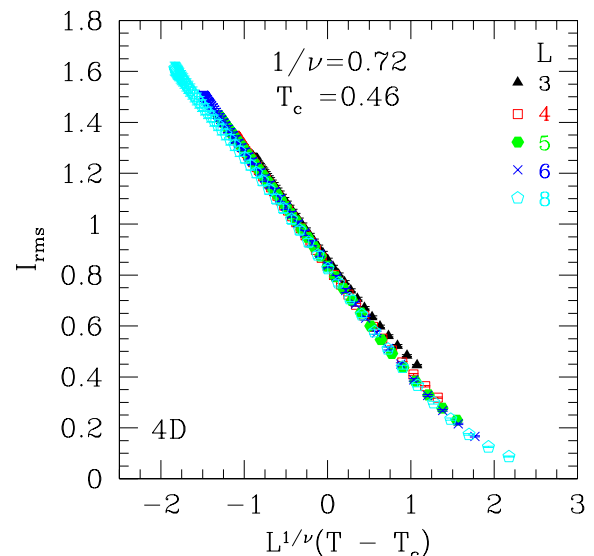


FIG. 12: Scaling of the root-mean-square current I_{rms} in three dimensions according to Eq. (11). We see acceptable scaling of the data around $T = 0.46$. Deviations at higher T are presumably due to corrections to scaling. This plot is for $1/\nu = 0.72$ and $T_c = 0.46$.

rect ordering temperature for the system, corrections to finite-size scaling being small for $L \geq 4$. The precision is limited mainly by the statistical error bars, as the curves for different sizes lie rather close together. A scaling plot of the root-mean-square current according to Eq. (11) is shown in Fig. 12 for $1/\nu = 0.72$ and $T_c = 0.46$.

B. Equilibrium Susceptibility

A log-log plot of the equilibrium susceptibility divided by L^2 as function of L for different temperatures is shown in Fig. 13. In absence of corrections to scaling this plot should be straight at T_c . We see that for $T > 0.46$ the data curve down, indicative that we are above the critical temperature. For $T < 0.46$ the data show a slight upward curvature, in agreement with $T < T_c$. Using Eq. 5 at $T = T_c$ we obtain $\eta = -0.47 \pm 0.02$ and a correction factor $\sim (1 - AL^{-\omega})$ with $\omega \approx 2.5$ and $A = 0.6$. For temperatures below T_c a higher effective $\eta(T)$ is obtained at each temperature and the correction factor appears to be temperature-independent. The correction term is almost negligible for $L \geq 4$; if we make straight line fits to $\ln[\chi(T)/L^2]$ against $\ln L$ for $L = 4$ to 8, we find χ^2 values which increase sharply above $T \approx 0.40$, and which rise slowly for temperatures below $T \approx 0.40$, Fig. 14.

In both Ising spin glasses and GGs the first term in the RG ϵ -expansion for the leading irrelevant operator is $\omega(d) \sim (6 - d)^{36,37}$ implying that ω will be high in dimension 3. High-temperature series expansion data show that ω is greater than 3 in dimension 3 for the ISG³⁸. If we make the plausible assumption that this is the case also for the GG, the leading correction term will be due to the lattice artifact so the correction factor is $[1 + AL^{-(2-\eta)}]$. Fits to all 3D GG $\chi(L, T)$ data from $L = 2$ to 8 using this correction factor give a clear minimum in χ^2 as a function of temperature at $T = 0.45 \pm 0.02$ (inset to Fig. 14), which we can identify with T_c . The effective exponent $\eta_{\text{eff}}(T)$ is shown in Fig. 16.

An overall scaling plot of $\chi(L, T)/L^{2-\eta}$ as a function of $L^{1/\nu}(T - T_c)$ for $L \geq 4$ is shown in Fig. 15. We estimate $1/\nu = 0.72 \pm 0.02$.

C. Binder parameter

In spin glasses the Binder parameter g defined in Eq. (7) is independent of system size at the transition temperature as it is proportional to a function which only depends on $L^{1/\nu}(T - T_c)$. Consequently different lines at different temperatures cross at T_c . In vector systems this is not the case: data for different system sizes splay for $T > T_c$ but not for $T < T_c$, as can be seen in Fig. 17. From the data one can, at best, estimate T_c roughly because the data do not cross. The same behavior is found in the three-dimensional XY spin glass³⁹. This has been ascribed to the ordering being chiral in this model. As no chirality can be defined for the gauge glass, this is not the case here and the behavior of g for the GG remains to be understood.

D. Correlation length

The data for the ratio $\xi_L(T)/L$ are shown in Fig. 18. As in four dimensions there are strong finite-size correc-

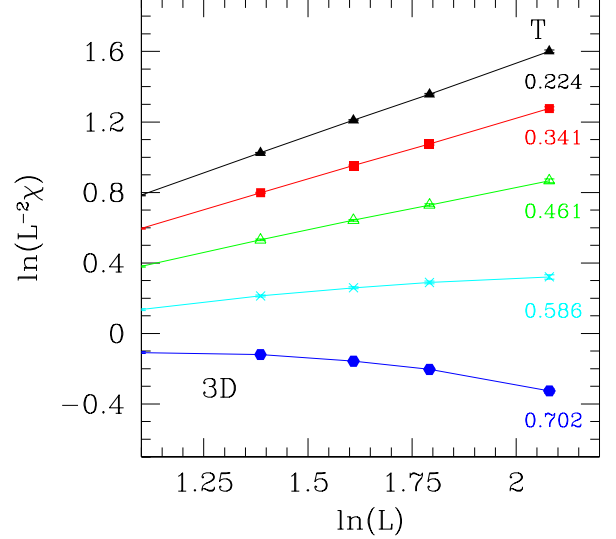


FIG. 13: Data for $\ln(\chi/L^2)$ vs $\ln L$ for different temperatures in three dimensions. The data show a change in curvature in the log-log plot while scanning through the T_c -estimate from the root-mean-square currents, 0.46. At T_c we expect $\chi \sim L^{2-\eta}$.

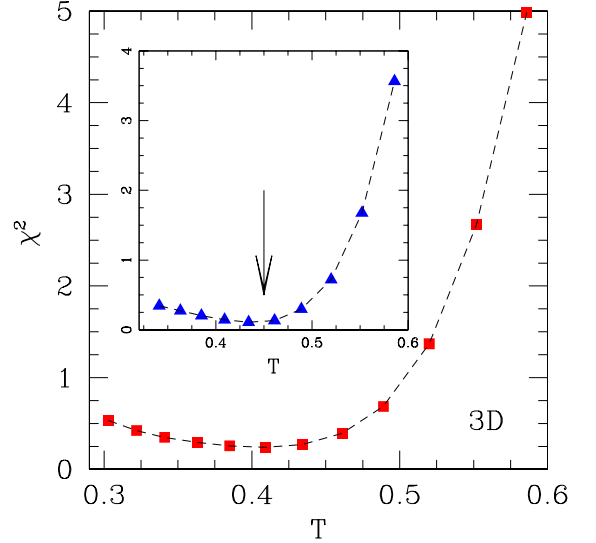


FIG. 14: χ^2 -deviation from a straight-line fit for the susceptibility data in three dimensions. The main panel shows data for a fit with no corrections to scaling due to lattice artifacts, whereas in the inset we show the data where corrections to scaling are included in the fits of $\ln(\chi/L^2)$. The data in the inset show a minimum at $T \approx 0.45$, in agreement with data from Ref. 6 and with the root-mean-square current estimate from Sec. VIA.

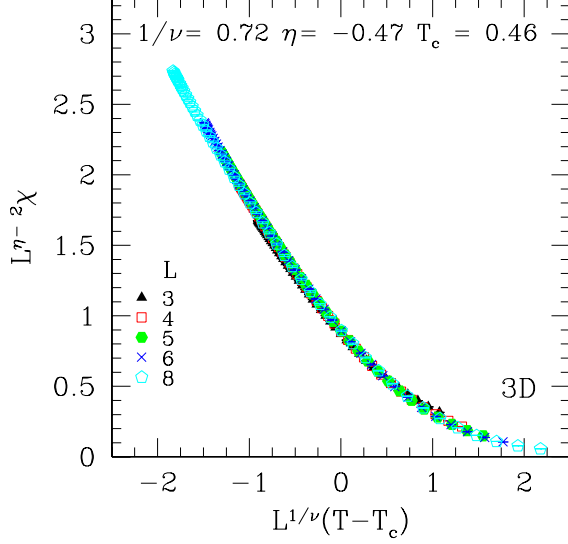


FIG. 15: Scaling plot according to Eq. (4) of the susceptibility data presented in Fig. 13 in three dimensions. Optimal scaling is obtained for $T_c \approx 0.46$, $1/\nu \approx 0.72$, and $\eta \approx -0.47$.

tion effects; in addition, the curves for different L lie close together. The intersections between curves for different L change with temperature in such a way that from these data alone it would be very hard to identify T_c to better than $T_c = 0.50 \pm 0.05$.

E. Non-equilibrium susceptibility

In just the same way as in four dimensions the non-equilibrium susceptibility is recorded for large system sizes, $L = 16$. The effective dynamical exponent $z(T)$ is estimated from the comparison of the time-dependent non-equilibrium susceptibility and the size-dependent equilibrium susceptibility, Fig. 19, and the effective dynamical critical exponent $z(T)$ is shown as a function of temperature in Fig. 20. At $T = 0.46$ we obtain $z(T) = 4.7 \pm 0.1$, in agreement with the results from Ref. 6 but with smaller error bars.

F. Autocorrelation function decay

Corrections to finite time scaling in three dimensions extend to times of the order of 100 MCS, limiting the precision of the measurement of the exponent $x(T)$, as in four dimensions. For this particular system the directly measured effective exponent $\eta(T)$ and the indirectly estimated $\eta^*(T)$ are very similar over a range of temperatures, as shown in Fig. 16. Hence it is not possible to obtain an independent measurement of T_c using the consistency criterion outlined above.

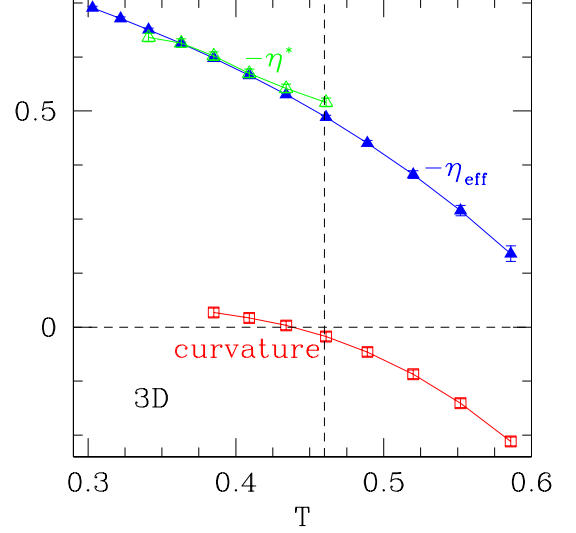


FIG. 16: Data for the effective exponent $\eta_{\text{eff}}(T)$ as a function of temperature in three dimensions. Also plotted η^* as estimated from off-equilibrium simulations. Both exponents do not cross cleanly making it difficult to determine T_c . The vertical dashed line marks our estimate for T_c , 0.46. Also shown is the curvature of the susceptibility data (see Fig. 13) from a second-order polynomial fit. The data cross zero curvature (horizontal dashed line) at $T = 0.44 \pm 0.01$, a value slightly lower than other estimates of T_c .

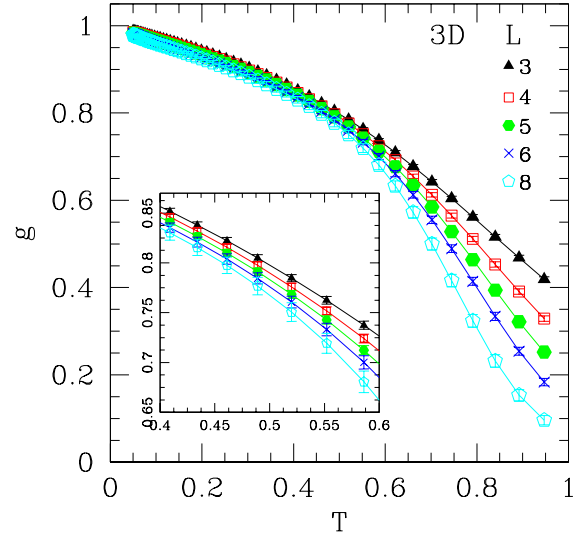


FIG. 17: Data for the Binder ratio g as a function of temperature for several system sizes. We see that the data do not cross for $T = T_c \approx 0.46$ and also do not splay for T smaller than T_c . The inset zooms into the region $T \leq 0.6$.

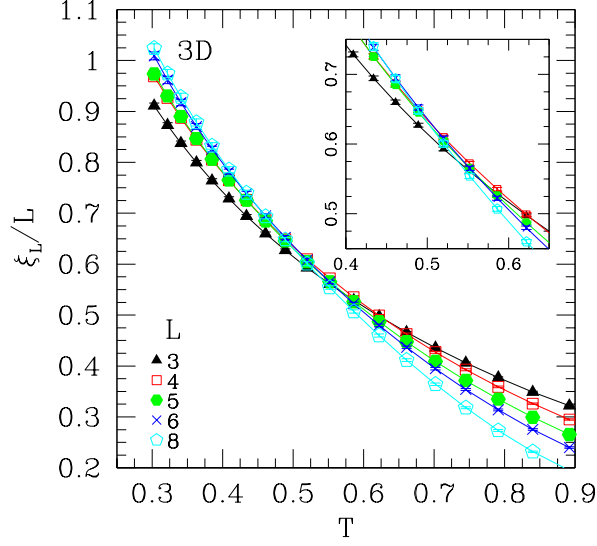


FIG. 18: Correlation length ξ_L divided by L for different system sizes in three dimensions. The data cross at $T \approx 0.5$ but only splay slightly making it difficult to give a precise estimate of the transition temperature.

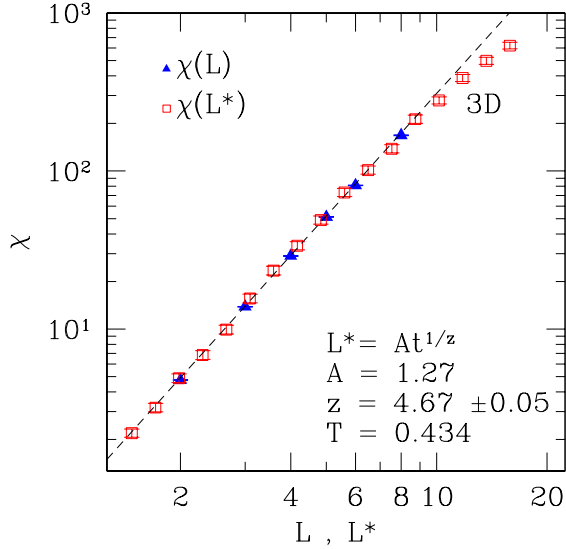


FIG. 19: Spin-glass susceptibility from equilibrium measurements $\chi(L)$ at $T = 0.434$ in three dimensions. $\chi(L^*)$ is the susceptibility determined from the off-equilibrium simulations with $L^* = A t^{1/z}$, $A = 1.27$, and $z \approx 4.67$. We choose L^* so that the data for $\chi(L)$ and $\chi(L^*)$ fall on a straight line allowing us to determine the dynamical critical effective exponent $z(T)$ as a function of temperature. When $L^*(t)$ approaches the sample size (here $L = 16$), $\chi(L^*)$ necessarily saturates. The dashed line is a guide to the eye.

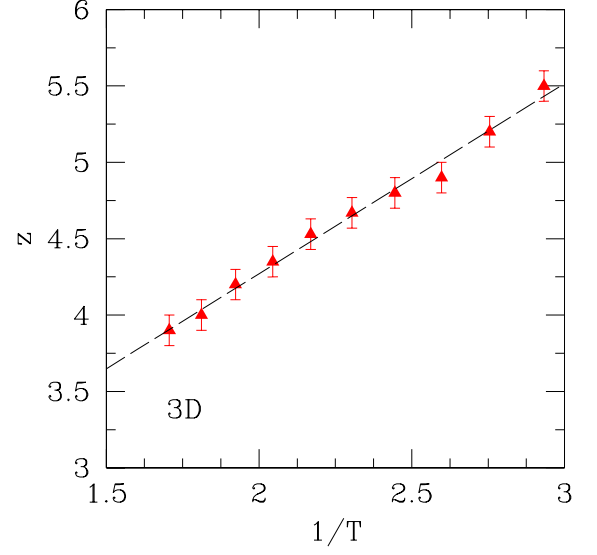


FIG. 20: Dynamical critical exponent z as a function of $1/T$ in three dimensions. For details see the text. The data are consistent with $z(T = T_c) = 4.7 \pm 0.1$, where the error is estimated by shifting the data until they visibly do not agree. The dashed line is a guide to the eye.

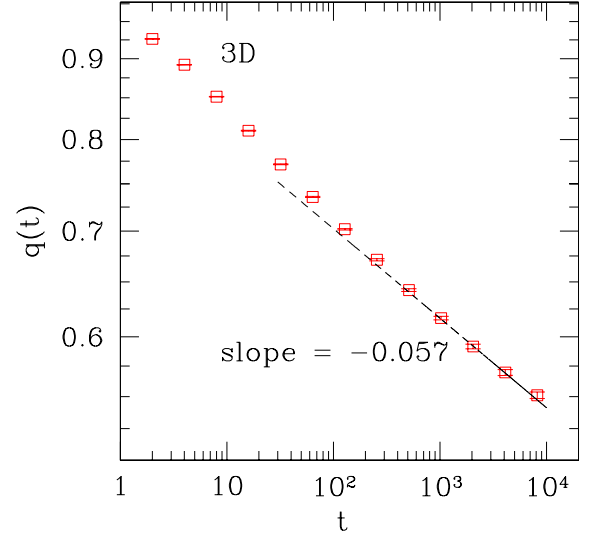


FIG. 21: Data for the autocorrelation function $q(t)$ in three dimensions as a function of time (measured in Monte Carlo steps). The dashed line is a guide to the eye to emphasize the asymptotic slope of $q(t)$ in a log-log plot.

VII. TWO DIMENSIONS

The gauge glass in two dimensions has been studied extensively in Refs. 7 and 11. In particular it was found that for this model $T_c = 0$, inferred from the values of critical exponents and several tests made. In this section we present results for off-equilibrium simulations, as well

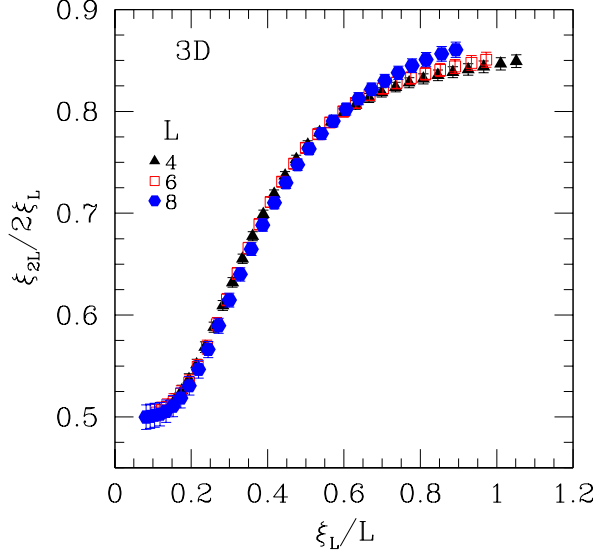


FIG. 22: Scaling plot of the data for $\xi_{2L}/2\xi_L$ vs ξ_L/L in two dimensions. The deviations at large ξ_L/L suggest corrections to scaling. If T_c is finite, the curves must go through $\xi_{2L}/2\xi_L = 1$ at $T = T_c$. The data only tend asymptotically to 1 proving that $T > T_c$.

as another test which shows that the system orders at zero temperature in two dimensions.

A. Correlation length

The GG in dimension two has been extensively studied^{5,7,16,40,41,42,43,44}. Measurements on various observables, in particular the correlation length, have established that the ordering temperature is either zero or much lower than our lowest measuring temperature, $T = 0.13$ ¹¹. In Fig. 22 we show correlation length data presented in the form of plots of the ratio $\xi(2L)/2\xi(L) \equiv \xi_{2L}/2\xi_L$ against $\xi(L)/L$. In the absence of corrections to scaling all points should fall on a single scaling curve, which for a finite ordering temperature should pass through $\xi(2L)/2\xi(L) = 1$ at $T = T_c$ [here $\xi(L)/L$ is independent of L]⁴⁵. For ordering which takes place only at zero temperature the ratio should tend asymptotically to a value which can be less than 1. The data show this form of behavior, demonstrating conclusively that for this system $T_c = 0$.

B. Non-equilibrium scaling

Measurements of the equilibrium susceptibility $\chi(L)$ for $L = 4$ to 16 (or to 24 above $T = 0.20$) and of the non-equilibrium susceptibility $\chi(t)$ for samples of size $L = 64$ are shown in Fig. 23. As for the other dimensions, the non-equilibrium data are scaled using $L^* = At^{1/z}$ with A and z chosen at each temperature so that the

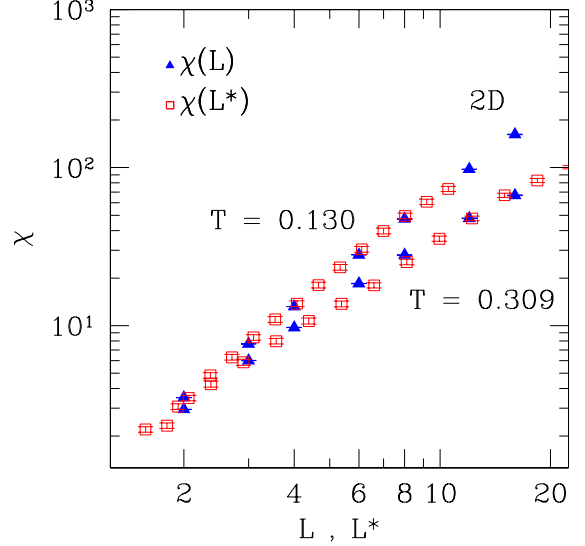


FIG. 23: Examples of excellent dynamic scaling well into the paramagnetic region in two dimensions. Spin-glass susceptibility from equilibrium measurements $\chi(L)$ (triangles) and $\chi(L^*)$ from scaled dynamical measurements (squares) at two temperatures: $T = 0.130$ (upper set of curves) and $T = 0.309$ (lower set of curves).

two sets of susceptibility data scale together. The scaling is particularly satisfactory because a wide range of L could be used for the equilibrium measurements, and because the non-equilibrium sample sizes have been chosen such that for all measurements L^* is much smaller than the sample size, so there are no saturation effects at long times. This demonstrates once again, but more clearly than for higher dimensions, that a dynamical exponent $z(T)$ can be defined relating the annealing time t to an effective length $L^*(t)$ for temperatures well above any critical temperature. The scaling holds to within the present statistical accuracy for the whole range of L from $L = 4$ to $L = 24$, or alternatively for anneal times from 2 MCS to over 16000 MCS. It appears that the dynamic scaling concept is ubiquitous and is not just valid at critical points. Finally, Fig. 24 shows data for the autocorrelation function $q(t)$. One can clearly see that the data, presented in a log-log plot, are strongly curved suggesting that the standard scaling functions for a finite-temperature transition do not apply.

VIII. COMPARISON OF TECHNIQUES

We can draw comparisons between the different techniques for estimating T_c and the critical exponents. It should be noted that equilibrium data for the different observables studied are taken within the same runs which allows a comparison of the relative statistical precision of the different measurements for exactly the same computational effort. As an example, for measurements made

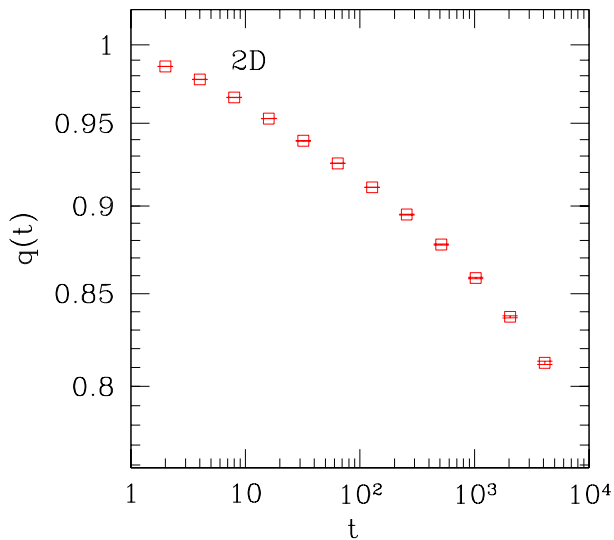


FIG. 24: Data for the autocorrelation function $q(t)$ in two dimensions as a function of time (measured in Monte Carlo steps). Here $L = 64$ and $T = 0.13$. The curvature of the log-log plot demonstrates yet again that any freezing is well below this temperature.

at $L = 8$ at $T = 0.461$ in dimension 3 and with the simulation parameters listed in Table II, the spin-glass susceptibility χ is accurate to 0.5%, the correlation length $\xi(L)$ to 0.7%, the current I_{rms} to 1.6% (and the internal energy to 0.02%) with the quoted errors purely statistical.

The major difficulty in the interpretation of the data is not statistics but corrections to scaling. In the gauge glass the current method turns out to be relatively insensitive to corrections to finite-size scaling and is therefore already reliable for relatively small samples. Averaging over large numbers of samples is however essential for these measurements because of strong intrinsic sample to sample fluctuations. In ISGs measurements of the critical behavior of the domain-wall stiffness (see for instance Ref. 46) could well provide an equally efficient and reliable method to estimate T_c , applicable quite generally.

Direct analysis of the spin-glass susceptibility $\chi(L, T)$ on its own is also reliable and efficient, particularly as the statistical precision of this parameter is high. At $T = T_c$ there is pure power-law behavior, $\chi(L, T)/L^2 \sim L^{-\eta(T)}$. The onset of deviations from the pure power-law behavior below and above the ordering temperature provides a clear signature for T_c .

In dimension four, even with the restricted range of L available, there is a downward deviation from the pure power law as soon as $T > T_c$, and an upward deviation from the pure power law for temperatures $T < T_c$. Corrections appear to be negligible as the straight line fit at T_c is excellent even for $L = 2$.

In dimension three the onset of deviation from a pure power law to a downward curvature at temperatures

above $T \sim 0.46$ gives a clear indication of T_c but the low-temperature upturn is weak. Corrections are present as there is a weak curvature at small L for all temperatures. If the plausible assumption is made that the leading correction to scaling is the leading analytic term, a precise estimate for T_c is obtained from fits using all the $\chi(L, T)$ data over the whole range of L . This estimate is consistent with the value from the current measurements.

The susceptibility method (see sections VB and VIB) becomes progressively more precise when data for larger samples are available. In the present case, data up to $L = 5$ only are sufficient for dimension 4, but in dimension 3 it would have been very helpful to have had data up to $L = 12$; with such data in hand it would be possible to pinpoint the transition temperature to even higher precision from susceptibility measurements alone.

The technique involving the consistency of observables deduced from non-equilibrium scaling and equilibrium susceptibility gives an estimate for T_c which has been found to be in excellent agreement with those obtained from the other methods for dimension 4. This despite the presence of short-time corrections to scaling in $q(t)$ that were unexpected. In dimension 3 consistency between alternative methods of estimating parameters holds over a range of temperatures rather than at a unique temperature which could be identified with T_c . This accidental consistency has not been observed in other systems and remains to be understood, but means that the technique in this particular case cannot be used to estimate T_c with any precision. The non-equilibrium measurements are relatively economical in computational resources as full thermodynamic equilibration is not required.

Estimates of T_c from the intersections of correlation length ratios $\xi(L)/L$ turn out to be misleading in dimension 4 because of strong intrinsic corrections to finite-size scaling for the small or moderate system sizes to which computational resources generally limit measurements in spin-glass systems at high dimensions. This parameter thus gives a qualitative indication that spin-glass ordering is occurring but it is not reliable for extracting precise values of the ordering temperature from small L data even in a situation where other measurements can give consistent and satisfactory estimates for an equivalent range of L . It can be noted that while corrections to finite-size scaling in measurements of $\chi(L)$ appear to be negligible for the GG in dimension 4, the corrections for $\xi(L)/L$ are still very strong at size $L = 5$. Even in dimension 3 where the corrections are weaker, this observable remains a poor tool for estimating the transition temperature. Strong correction effects in $\xi(L)/L$ can also be seen in data reported for XY spin glasses²¹ and have been found in certain ISGs. Therefore the correction effect appears to be generic and this technique should be applied only with caution.

Finally, estimates from the Binder parameter are inappropriate for the GG as the curves for different system sizes do not intersect for the range of L over which measurements are carried out. It is possible that there are

TABLE V: Critical temperature T_c and critical exponents for the GG in different space dimensions d and from different references. In the table KC represents results from this work, whereas RY represents Ref. 5 by Reger and Young, OY Ref. 6 by Olson and Young and K Ref. 11 by Katzgraber.

d	Ref.	T_c	η	ν	z	ω
4	RY ⁵	0.96(1)	–	0.70(15)	–	–
4	KC	0.89(1)	–0.74(3)	0.70(1)	4.50(5)	–
3	OY ⁶	0.47(3)	–0.47(7)	1.39(20)	4.2(6)	–
3	KC	0.460(15)	–0.47(2)	1.39(5)	4.7(1)	2.5(5)
2	K ¹¹	0	0	2.56(20)	∞	–

strong finite-size corrections for this parameter so that intersections would only be seen for much larger L .

Once T_c has been estimated, the susceptibility measurements at that temperature give immediately the corresponding value of the critical exponent η . The precision for this parameter is limited entirely by the accuracy with which T_c is known. The exponent ν is estimated from scaling plots of current data and from scaling plots of susceptibility data. Once again precision is limited by the accuracy with which T_c has been determined. The dynamical exponent z can be measured accurately from a comparison of equilibrium and non-equilibrium susceptibilities. The data show that $z(T)$ can be estimated operationally over a wide range of T including temperatures well above the ordering temperature [$z(T)$ varies continuously through the ordering temperature].

In the light of this extensive analysis, it would seem appropriate to critically re-assess the estimates for the critical exponents in the ISG family.

IX. CRITICAL PARAMETERS AS A FUNCTION OF SPACE DIMENSION

The critical parameters for the GG obtained from this and earlier work are listed in Table V.

In both dimensions 3 and 4 the GG ordering temperatures T_c are roughly half of those for the Gaussian ISG. By interpolation between the zero-temperature current stiffness exponents $\theta(d)$ in dimensions 1, 2 and 3¹², we can estimate the lower critical dimension for the GG as the dimension at which $\theta(d)$ passes through zero: $d_{\text{lcd}} \approx 2.5$, very similar to that of the ISG systems with continuous interaction distributions^{47,48} (see Table VI).

The corrections to scaling in the GG follow just the same pattern as in the bimodal ($\pm J$) ISGs. In the Gaussian ISG the corrections to scaling for $\chi(L)$ at T_c appear very weak and so unmeasurable. In dimension 4 for both cases the correction to scaling for the susceptibility $\chi(L)$ is so weak as to be unobservable even down to $L = 2$. In dimension 3 there is a clear correction to scaling for $\chi(L)$ which can be fitted satisfactorily to the form $\sim (1 + AL^{-\omega_{\text{eff}}})$. ω_{eff} in the ISG case has been interpreted as the leading irrelevant op-

TABLE VI: Critical temperature T_c and critical exponents for the ISG in different space dimensions d with Gaussian interactions. In the table PRR represents Ref. 49 by Parisi, Ricci-Tersenghi and Ruiz-Lorenzo, MPR Ref. 50 by Marinari, Parisi and Ruiz-Lorenzo, CEA Ref. 51 by Campbell *et al.*, and BY Ref. 52 by Bhatt and Young.

d	Ref.	T_c	η	ν	z
4	PRR ⁴⁹	1.80(1)	–0.35(5)	1.0(1)	–
4	CEA ⁵¹	1.78(1)	–0.48(2)	1.08(10)	4.9(4)
3	MPR ⁵⁰	0.95(4)	–0.36(6)	2.00(15)	–
3	CEA ⁵¹	0.92(2)	–0.42(3)	1.65(5)	6.45(10)
2	BY ⁵²	0	0	3.63(10)	–

erator correction¹⁸, and this could also be the case for the three-dimensional GG. However, it seems more likely that the correction is dominated by a “lattice artifact” giving $\omega_{\text{eff}} = 2 - \eta$, which has no relation to the leading irrelevant operator^{13,14}. For both the three-dimensional GG and the three-dimensional bimodal ISG, the value of the apparent correction to scaling exponent is compatible with this interpretation, which would imply that the leading irrelevant operator term has an exponent value $\omega > 2 - \eta$.

Finally, we can give an overview of the critical exponents in the GG and ISG families as a function of space dimension. It should be noted that there are some constraints that apply to both families: at the upper critical dimension $d = 6$, $\nu = 1/2$, $\eta = 0$, and $z = 4$. If $T_c = 0$, $\nu = 1/\theta$, where θ is the stiffness exponent. Therefore, at the lower critical dimension where the stiffness exponent $\theta = 0$, ν is infinite. For systems with a non-degenerate ground state (such as the GG or the ISG with Gaussian interactions, but not the ISG with bimodal interactions), when $T = 0$ there is no decay of the correlation function $G(r)$ with r . This necessarily implies that when $T_c = 0$, $\eta(d) \equiv 2 - d$. (For systems with degenerate ground states $\eta(d) > 2 - d$).

The leading terms in the RG ϵ -expansion for the GG are $\nu(d) = 1/2 + 5\epsilon/24$ and $\eta(d) = -\epsilon/6$. For the ISG $\nu(d) = 1/2 + 5\epsilon/12$ and $\eta(d) = -\epsilon/3$ ^{53,54}. It can be seen in Figs. 25 and 26, respectively, that in the GG as well as for the ISG the leading ϵ -expansion term gives the right sign and a qualitative indication of the strength of the variations of the exponents just below the upper critical dimension. The leading terms in the expansion for η cannot, however, be used to predict that the $\eta(d)$ values are much more negative in the GG than in the ISG. The observed exponents deviate strongly from the curves calculated to third order for the ISG where the second and third order expansion terms are very large. This deviation is smaller for the GG. The leading term in the ϵ -expansion for the exponent ν works better, with $\nu(d)$ being higher for the GG than for the ISG, in agreement with the relative strengths of the leading terms (including higher order terms would entirely destroy the agreement). This is all in striking contrast to the canonical

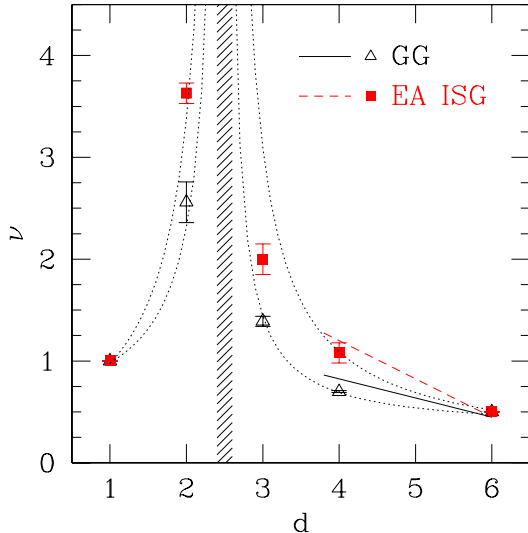


FIG. 25: Critical exponent ν as a function of space dimension for the ISG with Gaussian bonds and the GG (data taken from Tables VI and V, respectively). The shaded region denotes the area where one expects the lower critical dimension. The solid [dashed] line represents the RG ϵ -expansion estimate for the GG [ISG], as shown in the text, and the dotted lines are guides to the eye. At the lower critical dimension one expects $\nu(d \rightarrow d_{\text{lcd}}) \rightarrow \infty$. The data for the ISG and GG support this behavior.

ferromagnets (Ising, XY, or Heisenberg) without disorder, where the third order ϵ -expansion correction gives excellent predictions for $\eta(d)$ and $\nu(d)$.

If we look at the overall behavior of the exponents over the whole range of d , the shape of the $\nu(d)$ -curves is fairly similar for the GG and Gaussian ISG families, although the divergence at the lower critical dimension $d_{\text{lcd}} \approx 2.5$ is distinctly narrower in the GG case. The shapes of the $\eta(d)$ curves are on the other hand dramatically different. The leading terms in the ϵ -expansions agree poorly with the data even for $d = 4$, with an inversion of the measured positions of $\eta(d)$ as compared with the expansion predictions. For the Gaussian ISG family $\eta(d)$ decreases as the dimension drops from the upper critical dimension to the lower critical dimension. For the GG there is a deep minimum in $\eta(d)$ somewhere in the region of $d = 4$ (data at $d = 5$ would be needed to pin down the position of the minimum). In spin glasses, simply going from Ising to vector spins changes this exponent considerably, whereas in three-dimensional ferromagnets η is very small and practically independent of the type of spin symmetry.

Finally, in Fig. 27 the critical dynamical exponent $z(d)$ can be compared near $d = 6$ with the van Hove approximation $z = 2(2 - \eta)^{55}$ or for the ISG case with the first order ϵ -expansion $z = 2(2 - \eta)/(1 + \epsilon/4)^{56}$. The van Hove expression can provide a qualitative indication for $z(d)$ once the numerical values of $\eta(d)$ are known, but if

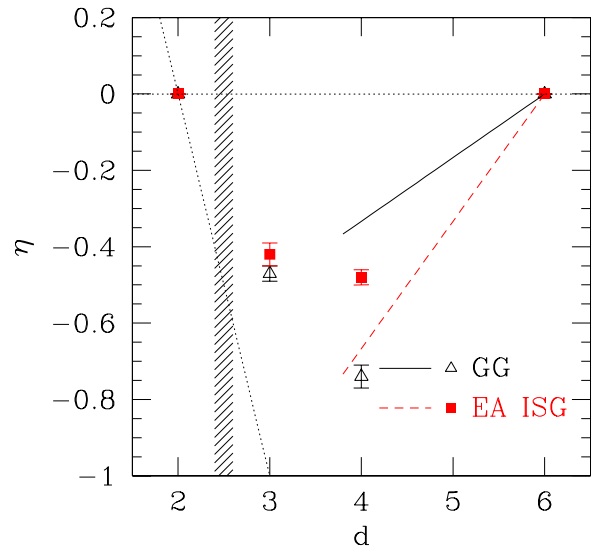


FIG. 26: Critical exponent η as a function of space dimension. The diagonal dotted line represents the physical limit line $\eta(d) = 2 - d$, whereas the horizontal dotted line represents $\eta = 0$. The solid and dashed lines represent the ϵ -expansion estimates for η for the GG and ISG, respectively. For all $d < d_{\text{lcd}} \approx 2.5$ $\eta(d)$ must join the limit line. The shaded region denotes the area where one expects the lower critical dimension.

the directly measured $\eta(d)$ values are used rather than the epsilon expansion estimates, this expression would predict higher z values at each d for the GG compared with the ISG values, which is not what is observed. $z(d)$ must diverge at the lower critical dimension, while curiously the GG $z(d)$ values only increase slightly between $d = 4$ and $d = 3$. For the Gaussian ISG, $z(d)$ shows an indication of divergence as the space dimension drops.

X. CONCLUDING REMARKS

We have studied the critical parameters of the GG, in dimensions 2, 3 and 4. The data confirm that T_c is zero in two dimensions. It appears that the most reliable and accurate methods for estimating critical temperature and exponent values are direct susceptibility measurements, effective stiffness measurements (current measurements in the GG case), and a combination of non-equilibrium and susceptibility measurements. In each case corrections to scaling are either so small as to be negligible or can be taken into account. Binder parameter measurements are inappropriate as the Binder parameter curves do not intersect, at least for the system sizes used, and correlation length measurements are not always reliable because there can be strong deviations from finite-size scaling.

From these results a general strategy for obtaining (high-precision) critical parameters numerically in any

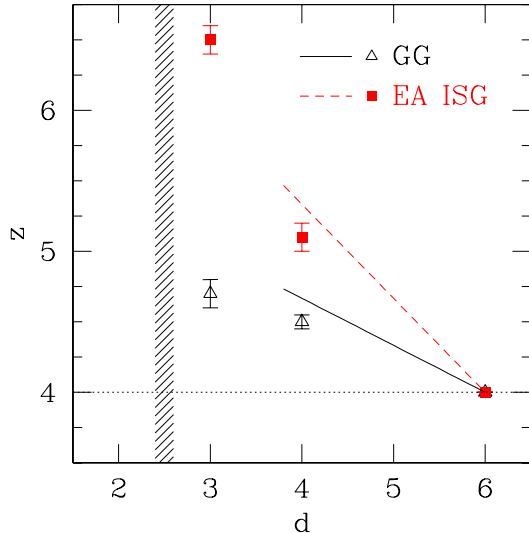


FIG. 27: Critical exponent z as a function of space dimension. The horizontal dotted line marks the mean-field asymptotic value $z = 4$, whereas the shaded region denotes the area where one expects the lower critical dimension. The solid [dashed] curve shows the asymptotic behavior as predicted from the van Hove approximation⁵⁵ for the GG [ISG]. One expects that $z(d \rightarrow d_{\text{lcd}}) \rightarrow \infty$. The ISG data show this behavior whereas the GG data are inconclusive.

glassy system can be sketched out. It is essential to be able to rely on high-quality equilibrium susceptibility data over a wide range of sizes and to as large a size as computational resources allow. Careful analysis of these data allowing for the leading correction to scaling term should provide reliable estimates of the ordering temperature and of the equilibrium critical exponents. Further measurements of the effective stiffness as a function of temperature together with non-equilibrium behavior can then confirm the value of the ordering temperature and give further information on other exponents including the critical dynamical exponent z . Parameters involving ratios (such as the Binder parameter or the correlation length) seem frequently to be biased, at small and moderate sizes, by complicated corrections to scaling and

should be treated with caution.

If we compare with other systems having $d = 6$ as upper critical dimension, ISGs and percolation, the exponent $\nu(d)$ always evolves regularly, diverging when the dimension reaches the lower critical dimension. The exponent $\eta(d)$ on the other hand changes dramatically in form from one family to the next. For the Gaussian ISG $\eta(d)$ grows smoothly more negative as the dimension drops from the upper critical dimension to the lower critical dimension. For the percolation systems $\eta(d)$ has a weak minimum around $d = 3$ before becoming positive at $d = 2$ ⁵⁷. The present results show that for the GG there is a deep minimum in $\eta(d)$ near $d = 4$. This is in stark contrast to the situation in the canonical Ising, XY, or Heisenberg systems with no disorder where $\eta(d)$ hardly changes at all when the degrees of freedom of the spin are modified. In addition, for the canonical systems the RG ϵ -expansion to third order gives excellent predictions for the exponents at dimensions well below the upper critical dimension, while for the ISG and GG systems the ϵ -expansion to the same order^{53,54} gives poor predictions for dimensions quite close to the upper critical dimension $d = 6$.

We have thus proposed a road plan for determining critical exponents reliably and accurately from simulations; however the results confirm once again that the canonical RG theory lacks essential ingredients when applied to glassy systems. The physical significance of the exponent values obtained, however good they are, must remain obscure until the appropriate theoretical approach going beyond the traditional RG is found for interpreting them.

Acknowledgments

We would like to thank J. Salas for helpful correspondence. C. De Dominicis and A. J. Bray kindly supplied us with the leading term for the exponent ω in the ϵ -expansion for the ISG and the GG cases, respectively. The simulations were performed on the Asgard cluster at ETH Zürich.

¹ C. de Dominicis, I. Kondor, and T. Temesári, *Beyond the sherrington-kirkpatrick model*, in *Spin Glasses and Random Fields*, edited by A. Young (World Scientific, Singapore, 1998).

² H. Kawamura, *Chiral ordering in Heisenberg spin glasses in two and three dimensions*, Phys. Rev. Lett. **68**, 3785 (1992).

³ H. Kawamura, *Dynamical Simulation of Spin-Glass and Chiral-Glass Orderings in Three-Dimensional Heisenberg spin glasses*, Phys. Rev. Lett. **80**, 5421 (1998).

⁴ J. D. Reger, T. A. Tokuyasu, A. P. Young, and M. P. A.

Fisher, *Vortex-glass transition in three dimensions*, Phys. Rev. B **44**, 7147 (1991).

⁵ J. D. Reger and A. P. Young, *Monte carlo study of a vortex glass model*, J. Phys. A **26**, 1067 (1993).

⁶ T. Olson and A. P. Young, *Finite temperature ordering in the three-dimensional gauge glass*, Phys. Rev. B **61**, 12467 (2000), (cond-mat/991229).

⁷ H. G. Katzgraber and A. P. Young, *Numerical studies of the two- and three-dimensional gauge glass at low temperature*, Phys. Rev. B **66**, 224507 (2002), (cond-mat/0205206).

- ⁸ K. Hukushima and K. Nemoto, *Exchange Monte Carlo method and application to spin glass simulations*, J. Phys. Soc. Jpn. **65**, 1604 (1996).
- ⁹ E. Marinari, *Optimized Monte Carlo methods*, in *Advances in Computer Simulation*, edited by J. Kertész and I. Kondor (Springer-Verlag, Berlin, 1998), p. 50, (cond-mat/9612010).
- ¹⁰ H. G. Katzgraber and A. P. Young, *Nature of the spin-glass state in the three-dimensional gauge glass*, Phys. Rev. B **64**, 104426 (2001), (cond-mat/0105077).
- ¹¹ H. G. Katzgraber, *On the existence of a finite-temperature transition in the two-dimensional gauge glass*, Phys. Rev. B **67**, 180402(R) (2003), (cond-mat/0305393).
- ¹² H. G. Katzgraber and A. P. Young, *Monte Carlo simulations of spin-glasses at low temperatures: Effects of free boundary conditions*, Phys. Rev. B **65**, 214402 (2002), (cond-mat/0108544).
- ¹³ J. Salas and A. D. Sokal, *Universal Amplitude Ratios in the Critical Two-Dimensional Ising Model on a Torus*, J. Stat. Phys. **98**, 551 (2000), (cond-mat/9904038).
- ¹⁴ J. Salas and A. D. Sokal, *The 3-State Square-Lattice Potts Antiferromagnet at Zero Temperature*, J. Stat. Phys. **92**, 729 (1998).
- ¹⁵ H. G. Ballesteros, L. Fernandez, V. Martin-Mayor, G. Parisi, and J. J. Ruiz-Lorenzo, *Scaling corrections: site percolation and Ising model in three dimensions*, J. Phys. A **32**, 1 (1999).
- ¹⁶ K. Binder, *Critical properties from Monte Carlo coarse graining and renormalization*, Phys. Rev. Lett. **47**, 693 (1981).
- ¹⁷ H. Kawamura, *Simulation studies on the stability of the vortex-glass order*, J. Phys. Soc. Jpn. **69**, 29 (2000).
- ¹⁸ P. O. Mari and I. A. Campbell, *The ordering temperature and critical exponents of the bimodal Ising spin glass in dimension three*, Phys. Rev. B **65**, 184409 (2002).
- ¹⁹ L. Berthier and J. P. Bouchaud, *Geometrical aspects of aging and rejuvenation in the Ising spin glass: A numerical study*, Phys. Rev. B **66**, 054404 (2002).
- ²⁰ H. G. Ballesteros, A. Cruz, L. Fernandez, V. Martin-Mayor, J. Pech, J. J. Ruiz-Lorenzo, A. Tarancon, P. Tellez, C. L. Ullod, and C. Ungil, *Critical behavior of the three-dimensional Ising spin glass*, Phys. Rev. B **62**, 14237 (2000), (cond-mat/0006211).
- ²¹ L. W. Lee and A. P. Young, *Single spin- and chiral-glass transition in vector spin glasses in three dimensions*, Phys. Rev. Lett. **90**, 227203 (2003), (cond-mat/0302371).
- ²² F. Cooper, B. Freedman, and D. Preston, *Solving $\phi_{1,2}^4$ theory with Monte Carlo*, Nucl. Phys. B **210**, 210 (1982).
- ²³ V. Martin-Mayor, A. Pelissetto, and E. Vicari, *Critical structure factor in Ising systems*, Phys. Rev. E **66**, 26112 (2002).
- ²⁴ J.-K. Kim, A. J. F. de Souza, and D. P. Landau, *Numerical computation of finite size scaling functions: an alternative approach to finite size scaling*, Phys. Rev. E **54**, 2291 (1996).
- ²⁵ M. Palassini and A. P. Young, *Triviality of the ground state structure in Ising spin glasses*, Phys. Rev. Lett. **83**, 5126 (1999), (cond-mat/9906323).
- ²⁶ H. G. Katzgraber and I. A. Campbell, *Size-dependence of the Internal Energy in Ising and Vector Spin Glasses* (2003), in preparation.
- ²⁷ D. A. Huse, *Remanent magnetization decay at the spin-glass critical point: A new dynamic critical exponent for nonequilibrium autocorrelations*, Phys. Rev. B **40**, 304 (1989).
- ²⁸ G. Parisi, F. Ricci-Tersenghi, and J. J. Ruiz-Lorenzo, *Universality in the off-equilibrium critical dynamics of the three-dimensional diluted Ising model*, Phys. Rev. E **60**, 5198 (1999).
- ²⁹ R. E. Blundell, K. Humayun, and A. J. Bray, *Dynamic exponent of the 3D Ising spin glass*, J. Phys. A **25**, L733 (1992).
- ³⁰ E. Marinari and G. Parisi, *On the effects of changing the boundary conditions on the ground state of Ising spin glasses*, Phys. Rev. B **62**, 11677 (2000).
- ³¹ H. Rieger, *Nonequilibrium dynamics and aging in the three-dimensional Ising spin-glass model*, J. Phys. A **26**, L615 (1993).
- ³² Y. Ozeki and N. Ito, *Nonequilibrium relaxation study of Ising spin glass models*, Phys. Rev. B **64**, 024416 (2001).
- ³³ A. T. Ogielski, *Dynamics of three-dimensional Ising spin glasses in thermal equilibrium*, Phys. Rev. B **32**, 7384 (1985).
- ³⁴ J. Kisker, L. Santen, M. Schreckenberg, and H. Rieger, *Off-equilibrium dynamics in finite-dimensional spin-glass models*, Phys. Rev. B **53**, 6418 (1996).
- ³⁵ L. W. Bernardi, S. Prakash, and I. A. Campbell, *Ordering Temperatures and Critical Exponents in Ising Spin Glasses*, Phys. Rev. Lett. **77**, 2798 (1996).
- ³⁶ C. de Dominicis, private communication.
- ³⁷ A. J. Bray, private communication.
- ³⁸ L. Klein, J. Adler, A. Aharony, A. B. Harris, and Y. Meir, *Series expansions for the Ising spin glass in general dimension*, Phys. Rev. B **43**, 11249 (1991).
- ³⁹ H. Kawamura and M. S. Li, *Nature of the ordering of the three-dimensional XY spin glass* (2001), (cond-mat/0106551).
- ⁴⁰ M. P. A. Fisher, T. A. Tokuyasu, and A. P. Young, *Vortex variable-range-hopping resistivity in superconducting films*, Phys. Rev. Lett. **66**, 2931 (1991).
- ⁴¹ M. J. P. Gingras, *Numerical study of vortex-glass order in random-superconductor and related spin-glass models*, Phys. Rev. B **45**, 7547 (1992).
- ⁴² N. Akino and J. M. Kosterlitz, *Domain wall renormalization group study of xy model with quenched random phase shifts*, Phys. Rev. B **66**, 054536 (2002), (cond-mat/0203299).
- ⁴³ M. V. Simkin, *Comment on "Voltage-Current Characteristics of the Two-Dimensional Gauge Glass Model"* (1996), (cond-mat/9604178).
- ⁴⁴ E. Granato, *Current-voltage scaling of chiral and gauge-glass models of two-dimensional superconductors*, Phys. Rev. B **58**, 11161 (1998).
- ⁴⁵ M. Palassini and S. Caracciolo, *Universal Finite-Size Scaling Functions in the 3D Ising Spin Glass*, Phys. Rev. Lett. **82**, 5128 (1999).
- ⁴⁶ K. Hukushima, *Domain-wall free energy of spin-glass models: Numerical method and boundary conditions*, Phys. Rev. E **60**, 3606 (1999).
- ⁴⁷ J.-P. Bouchaud, F. Krzakala, and O. Martin, *Energy exponents and corrections to scaling in Ising spin glasses* (2002), (cond-mat/0212070).
- ⁴⁸ Note that for the upper critical dimension, $d = 6$, we expect mean-field exponents, i.e., $\nu = 1/2$, $\eta = 0$, and $z = 4$.
- ⁴⁹ G. Parisi, F. Ricci-Tersenghi, and J. J. Ruiz-Lorenzo, *Equilibrium and off-equilibrium simulations of the 4d Gaussian spin glass*, J. Phys. A **29**, 7943 (1996).
- ⁵⁰ E. Marinari, G. Parisi, and J. J. Ruiz-Lorenzo, *On the*

- phase structure of the 3d Edwards Anderson spin glass*, Phys. Rev. B **58**, 14852 (1998).
- ⁵¹ I. A. Campbell, D. Petit, P. O. Mari, and L. W. Bernardi, *Critical exponents in Spin Glasses : numerics and experiments*, J. Phys. Soc. Jap. **69 suppl A**, 186 (2000).
- ⁵² R. N. Bhatt and A. P. Young, *Numerical studies of Ising spin glasses in two, three and four dimensions*, Phys. Rev. B **37**, 5606 (1988).
- ⁵³ J. E. Green, *Critical behaviour of a random m-vector model*, J. Phys. A **17**, L43 (1985).
- ⁵⁴ M. A. Moore and S. Murphy, *Critical exponents of the vortex glass to order ϵ^3* , Phys. Rev. B **42**, 2587 (1990).
- ⁵⁵ A. Zippelius, *Critical dynamics of spin-glasses*, Phys. Rev. B **29**, 2717 (1984).
- ⁵⁶ G. Parisi and P. Ranieri, *One-loop contribution to the dynamical exponents in spin glasses*, J. Phys. A **30**, L415 (1997), (cond-mat/9701160).
- ⁵⁷ J. Adler, A. Meir, A. Aharony, and A. B. Harris, *Series study of percolation moments in general dimension*, Phys. Rev. B **41**, 9183 (1990).